ADVANCING EARTH AND SPACE SCIENCES

Paleoceanography and Paleoclimatology

RESEARCH ARTICLE

10.1029/2026PA005582

Antarctic, Southern Ocean, and Global Ocean Temperatures During Dansgaard–Oeschger Events

John Slattery[1,2], Louise C. Sime[1], Xu Zhang[1], Irene Malmierca-Vallet[1], and Francesco Muschitiello[2,3]

[1]Ice Dynamics and Paleoclimate, British Antarctic Survey, Cambridge, UK, [2]Department of Geography, University of Cambridge, Cambridge, UK, [3]Department of Applied Mathematics and Theoretical Physics, Centre for Climate Repair, University of Cambridge, Cambridge, UK

Key Points:

- Model simulations of Dansgaard–Oeschger (DO) events show that Antarctic, Southern Ocean, and Global Ocean temperatures are strongly linked
- Model mean changes generally agree well with proxy records of DO events following stadials that do not contain Heinrich events
- We combine proxy and model evidence to estimate likely ranges for the Global Mean Ocean Temperature changes of DO events

Correspondence to:

J. Slattery,
johatt11@bas.ac.uk

Citation:

Slattery, J., Sime, L. C., Zhang, X., Malmierca-Vallet, I., & Muschitiello, F. (2026). Antarctic, Southern Ocean, and Global Ocean temperatures during Dansgaard–Oeschger events. *Paleoceanography and Paleoclimatology*, *41*, e2026PA005582. https://doi.org/10.1029/2026PA005582

Received 8 JUN 2026
Accepted 12 AUG 2026

Author Contributions:

Conceptualization: Louise C. Sime, Francesco Muschitiello
Data curation: Xu Zhang, Irene Malmierca-Vallet
Formal analysis: John Slattery
Supervision: Louise C. Sime, Francesco Muschitiello
Visualization: John Slattery
Writing – original draft: John Slattery
Writing – review & editing: John Slattery, Louise C. Sime, Xu Zhang, Irene Malmierca-Vallet, Francesco Muschitiello

Abstract Global Mean Ocean Temperature (GMOT) changes are thought to be both an important consequence and a possible cause of Dansgaard–Oeschger (DO) events, a series of abrupt climate changes during the last glacial. Despite extensive reconstructions of GMOT from ice cores for other periods, no reliable reconstructions exist for Marine Isotope Stage 3, when DO events were most common. We investigate model simulations showing unforced DO-like oscillations alongside existing proxy reconstructions of Southern Ocean and Antarctic temperatures, which we show to be strongly linked to GMOT in the models though with consistently larger changes in Antarctic temperature than GMOT. We find that the models reproduce DO events following non-Heinrich stadials well, but that the GMOT changes they show across these events are comparable to the measurement error for ice core GMOT reconstructions and so would be difficult to detect. The simulations we use, which are not forced by Heinrich meltwater, do not capture the larger Southern Ocean and Antarctic warming associated with DO events that follow Heinrich stadials, making extrapolating our results to these events challenging. Additionally, there is a statistically robust disagreement between the proxies and models regarding the relative warming in Antarctica and the Southern Ocean, which adds further uncertainty to our estimates of GMOT warming. Nonetheless, we find that the GMOT changes across these larger DO events in MIS3 would be detectable. Given the importance of GMOT for understanding DO events, these should therefore be priority targets for future efforts to reconstruct GMOT from ice cores.

1. Introduction

Dansgaard–Oeschger events, or DO events, were a series of abrupt climate changes that took place during past cold climates (Dansgaard et al., 1993), and which are recorded in Greenland ice cores as rapid warming transitions from cooler stadial periods to warmer interstadial periods (Kindler et al., 2014; North Greenland Ice Core Project Members, 2004). They occurred most frequently during Marine Isotope Stage 3 (MIS3, Rasmussen et al., 2014) between 57 and 29 ka (Lisiecki & Raymo, 2005). Some MIS3 DO events were preceded by huge pulses of freshwater into the North Atlantic from the Laurentide Ice Sheet known as Heinrich events (Hemming, 2004). These DO events following Heinrich events were especially large, for example, showing greater warming in North Atlantic Sea Surface Temperature (SST) in both proxy records and model simulations (Pedro et al., 2022).

A growing body of evidence suggests that DO events may have been unforced internal oscillations governed by feedbacks in the coupled atmosphere-ocean-sea ice system (e.g., Li & Born, 2019; Malmierca-Vallet et al., 2023). Six different General Circulation Models (GCMs) so far can simulate spontaneous millennial-scale oscillations that are DO-like in nature under some combination of full glacial, mid-glacial, and pre-industrial background conditions (i.e., ice sheets, orbital parameters, and greenhouse gases; Malmierca-Vallet et al., 2023), with background conditions roughly matching those found during MIS3 being particularly conducive to such oscillations (Malmierca-Vallet et al., 2023, 2024). The proposed dynamics for the oscillations in each of these models tend to be rather similar, however the strengths of the various feedbacks differ between models and simulated events (Malmierca-Vallet et al., 2023), meaning that we still do not have a clear view of whether these models are correctly capturing the essential dynamics that seem to govern DO behaviors.

Although the strengths of the feedbacks that govern crucial DO dynamics and the nature of possible tipping events remain debated (Capron et al., 2021; Lynch-Stieglitz, 2017), DO warming events are clearly strongly associated with transitions from weak to strong states of the Atlantic Meridional Overturning Circulation or AMOC (Henry et al., 2016; Lynch-Stieglitz, 2017). By transporting vast quantities of heat northwards, the AMOC plays a key role in mediating the relationship betweens the climates of the Northern and Southern high latitudes (Pedro et al., 2018; Stocker & Johnsen, 2003). Antarctic ice cores record a temperature peak, known as an Antarctic Isotope Maximum (AIM), corresponding to every DO event in the Greenland cores (EPICA Community Members, 2006). The thermal bipolar seesaw hypothesis, first presented by Stocker and Johnsen (2003), explains this relationship by invoking an ocean heat reservoir, suggested to be the Southern Ocean, that is closely coupled to the Antarctic climate and controlled by variations in the AMOC strength. This heat reservoir depletes during Greenland Interstadials due to the increased northward heat transport by a strong AMOC and refills during Greenland Stadials when a weaker AMOC transports less heat.

Through climate model experiments, Pedro et al. (2018) find that the heat reservoir is not in fact the Southern Ocean, as suggested by Stocker and Johnsen (2003), but instead the interior (i.e., intermediate and deep waters) of the global ocean north of the Antarctic Circumpolar Current (ACC). The state of this heat reservoir can thus be characterized by variations in the volume-weighted Global Mean Ocean Temperature (GMOT). Understanding how GMOT varied across DO events is therefore a key component of our overall understanding of the processes by which these events impacted the global climate, and accurately reproducing these variations also represents an important test of the accuracy of climate model simulations of DO events. This is especially important given that DO events are often considered examples of climate tipping points (e.g., Vettoretti et al., 2026) and studied as analogs for potential future abrupt AMOC changes. Furthermore, subsurface ocean warming in the North Atlantic is also a likely required precursor to DO warming events as part of a self-sustaining thermohaline oscillation (Brown & Galbraith, 2016; Kuniyoshi et al., 2022; Malmierca-Vallet et al., 2023), meaning that GMOT change is not only a consequence of DO events but probably also partially reflects a required slow feedback for the generation of further DO events.

Previous analysis of model simulations of the Last Glacial Maximum (LGM) and the Pre-Industrial (PI) has found that GMOT is particularly strongly linked to SST in the Southern Ocean just north of the ACC, in the band between 30°S and 60°S (C. Zhu et al., 2024). This is because this latitude band of the Southern Ocean ventilates Antarctic Intermediate Water (AAIW), which is globally distributed and occupies a large proportion of the volume of the global ocean interior. Changes in the temperature of AAIW thus have a large impact on GMOT, and so changes in GMOT closely correlate with SST changes in this region where AAIW is ventilated (C. Zhu et al., 2024). By contrast, reorganizations of the deep water masses North Atlantic Deep Water (NADW) and Antarctic Bottom Water (AABW) are thought to have much more limited impacts on GMOT because NADW and AABW have similar average temperatures, and as one expands the other typically contracts (C. Zhu et al., 2024). These two properties combined mean that deep water reorganizations are expected to cause only very small net changes in GMOT, although these water masses nonetheless form part of the global ocean interior heat reservoir as they are influenced by downward heat flux from the AAIW above (C. Zhu et al., 2024). Freshwater-forced simulations of AMOC weakening show that, after heat accumulates in the Southern Ocean north of the ACC, increased eddy-heat transport across the ACC then causes warming in Antarctica that is additionally amplified by sea-ice loss (Pedro et al., 2018; C. Zhu et al., 2022). Combined, these results imply that GMOT, SST_{SO}, and Antarctic Temperature ($T_{Antarctic}$) should all be correlated, albeit with time lags due to the slow propagation of signals in the ocean and especially across the ACC.

GMOT has been extensively reconstructed for the last glacial cycle and beyond using measurements of noble gases preserved in ice cores (e.g., Baggenstos et al., 2019; Bereiter et al., 2018; Shackleton et al., 2019). This has revealed a strong correlation between changes in GMOT and those in Antarctic temperature proxies (Shackleton et al., 2021), just as predicted by model simulations. There is also proxy evidence from deglaciations for the expected link between millennial-scale changes in GMOT and AMOC (Grimmer et al., 2025), and for MIS3 DO events in particular a correlation between SST_{SO} and $T_{Antarctic}$ has been demonstrated from proxy records (Anderson et al., 2021). All in all, the dynamics identified in models therefore seem well-supported by proxy evidence. There is, however, a missing link in this picture, as despite the numerous reconstructions for other periods the GMOT changes during MIS3 remain poorly understood, with no reliable ice core-derived reconstructions for this period. So, whilst it might be expected that GMOT followed the pattern of $T_{Antarctic}$ changes across DO events, with GMOT peaks approximately simultaneous with DO events in Greenland, this cannot yet be confirmed. Whether and how GMOT changed across DO events in MIS3, as well as what its links were to Southern Ocean and Antarctic temperatures, therefore remain important unanswered questions.

In this study, we use climate model simulations showing spontaneous DO-like oscillations to investigate how GMOT might have varied across DO events. We further compare these model simulations to previously published proxy compilations of Southern Ocean and Antarctic temperatures, and assess the links between GMOT, SST_{SO}, and $T_{Antarctic}$. We finally comment on whether ice core reconstructions of MIS3 GMOT would be able to capture the signal of the changes associated with DO events, based on what we learn from the model simulations and existing proxy data.

2. Methods and Materials

2.1. Southern Ocean Temperature Records

Anderson et al. (2021) compile 14 SST reconstructions from 13 Southern Ocean cores situated between 30°S and 60°S which resolve changes across DO events during MIS3. The most common proxy type is alkenone ($U^{k'}{}_{37}$), but the compilation also includes reconstructions from Mg/Ca and assemblages. The authors reconstruct SST from all alkenone proxies in a consistent manner using the Sikes and Sicre (2002) field calibration. The Southern Ocean reconstructions integrate temperature from October to April (Sikes & Volkman, 1993; Ternois et al., 1998), and so they should be considered as reflecting summer SST in a broad sense. This matches both the seasonality of the highest alkenone fluxes in this region (Sikes et al., 2005; Ternois et al., 1998) and the seasonality of the assemblage-based SST reconstructions (Cortese & Abelmann, 2002; Crosta et al., 2004).

Anderson et al. (2021) create consistent chronologies for the 13 cores in their compilation by assuming that peaks in the SST reconstructions correlate with AIM events in an Antarctic ice core record. The 13 individual reconstructions are highly noisy, and so we focus on the stack of SST_{SO} that Anderson et al. (2021) also present, which has a greater signal/noise ratio. This stack is produced by taking anomalies for each reconstruction with respect to the MIS3 mean, binning the data points into 500-year bins, and then taking the average across each of the reconstructions with at least one data point in that bin. We calculate the warming associated with each AIM in the same manner as Anderson et al. (2021), described in Section 2.4, and also investigate potential bias in Appendix A.

2.2. Antarctic Temperature Records

To investigate changes in $T_{Antarctic}$, we make use of the Parrenin et al. (2013b) stack, calculated using water isotope data from the Epica Dome C (EDC), Dome Fuji, Epica Dronning Maud Land (EDML), Vostok, and Talos Dome ice cores in East Antarctic, after correcting for the impact of changes in seawater isotopes. Although more recent temperature reconstructions exist for some core sites (e.g., Landais et al., 2021) that are more thorough in distinguishing between changes in source and site temperature, the Parrenin et al. (2013b) stack is advantageous for proxy-model comparison because it includes a greater number of ice cores and so better reflects the Antarctic-mean, rather than ice core site-specific, temperature changes.

2.3. Climate Model Simulations

Reflecting the emerging view that DO events are unforced, internal oscillations, we investigate GMOT changes in simulations from four general circulation models which have been previously shown to reproduce spontaneous DO-like oscillations without external forcing (Malmierca-Vallet et al., 2023). We consider simulations from the models CCSM4 (Vettoretti et al., 2022), HadCM3 (Armstrong et al., 2022), MPI-ESM (Klockmann et al., 2018, 2020), and COSMOS (Zhang et al., 2021). Each of these models uses a different combination of full-glacial, mid-glacial, and pre-industrial background conditions. Furthermore, for all models other than COSMOS we have multiple simulations which differ only in their (fixed) CO_2 concentrations. For a full list of the simulations utilized and their background conditions, see Table 1.

Abrupt warming (cooling) transitions are identified in these simulations using the simulated temperature at the NGRIP Greenland ice core site, denoted T_{NGRIP}. Each transition is identified as the time when the temperature difference between the means of two adjacent sliding windows reaches a local maximum (minimum), and when the magnitude of this difference is also above a certain threshold. With appropriate window durations and threshold values for each model, this simple approach allows us to robustly separate simulated time into stadial periods with cooler T_{NGRIP} and interstadial periods with warmer T_{NGRIP}. Comparing T_{NGRIP} to GMOT for an example simulation in each model (Figure 1) we find that GMOT gradually warms during stadials and gradually

Table 1
Spontaneously-Oscillating Simulations Used in This Study

Model	Orbit (ka)	Ice sheets (ka)	CO_2 (ppm)	Length (yr)	Number of Stadials
Standard Simulations					
CCSM4	21	21	185	10,000	2
	21	21	200	8,000	2
	21	21	210	8,000	3
	21	21	220	8,000	3
	21	21	225	8,000	3
	21	21	230	10,000	1
HadCM3	30	30	190	4,700	2
	30	30	210	5,500	3
MPI-ESM	21	PI	195	8,000	4
	21	PI	206	12,350	5
	21	PI	217	8,000	6
COSMOS	34	40	195	5,000	4
Isotope-enabled Simulations					
HadCM3	30	30	200	2,000	1
COSMOS	34	40	195	5,000	4

Note. The standard simulations are used to investigate temperature changes, whilst the isotope-enabled simulations are used to calculate the palaeothermometer gradient. Note that the same COSMOS simulation is used for both purposes.

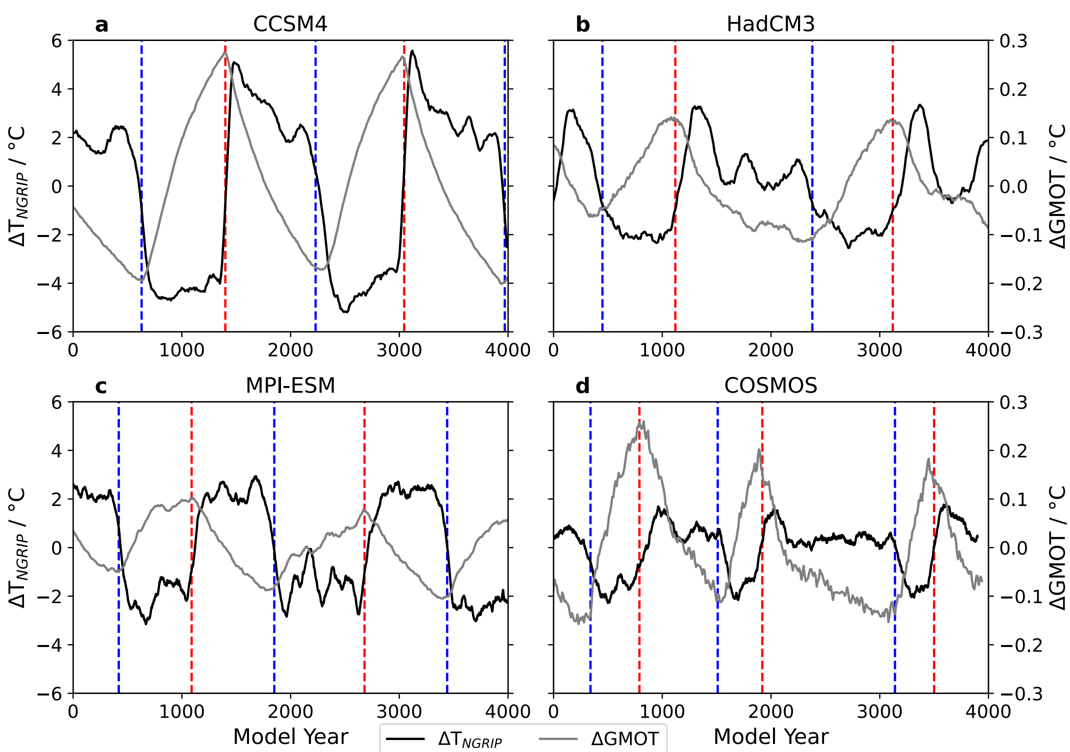

Figure 1. 100-year rolling average T_{NGRIP} (black) and 10-year rolling average GMOT (gray) anomalies for 4,000-year sections of single example simulations from each of the CCSM4 (a), HadCM3 (b), MPI-ESM (c), and COSMOS (d) models. Abrupt Greenland warming (cooling) transitions, as determined from T_{NGRIP}, are shown as dashed vertical red (blue) lines. We apply a 100-year rolling average for T_{NGRIP}, as opposed to the 10-year rolling average for GMOT, simply because T_{NGRIP} is inherently noisier and so requires a greater level of smoothing to make the millennial-scale variability clear.

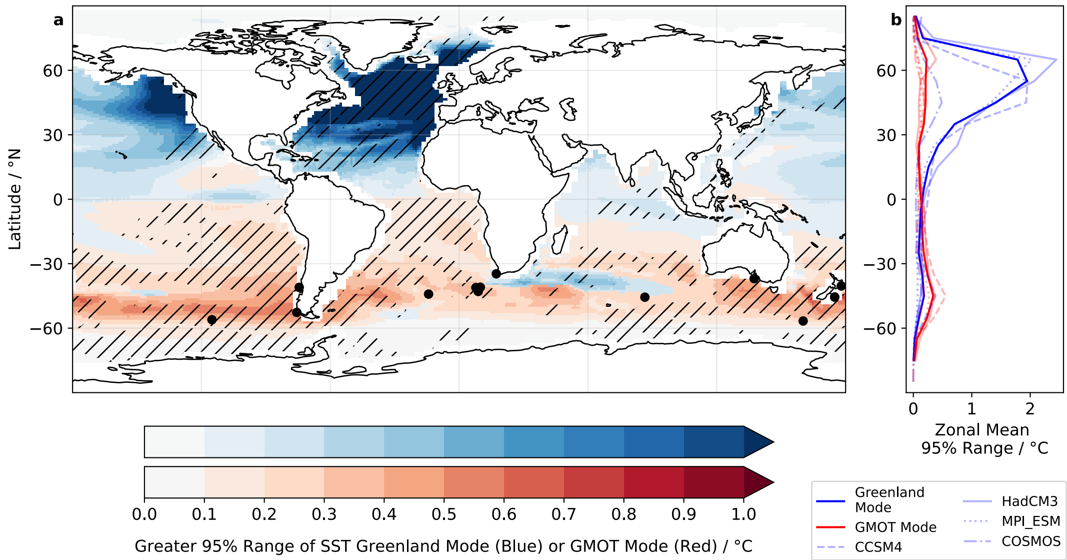

Figure 2. (a) Multi-model mean 95% range for SST Greenland mode (blue) or GMOT mode (red), whichever is greater. Hatching shows where all four models agree on which mode is dominant. Black dots show sediment core sites in the Anderson et al. (2021) compilation. (b) Zonal means for the SST Greenland mode and GMOT mode in both the multi-model mean (bolder lines) and each model separately.

cools during interstadials, following the expected behavior from the bipolar seesaw (Pedro et al., 2018). Peaks in GMOT thus approximately align with abrupt warming transitions in Greenland, and troughs in GMOT with abrupt cooling transitions in Greenland.

To identify areas where existing SST proxy records could provide an indication of GMOT changes, we decompose the grid cell SST in each simulation into a "Greenland Mode" with rapid changes and a "GMOT Mode" with gradual changes by regressing against T_{NGRIP} and GMOT, respectively. We then calculate the 95% range of each of these two modes in order to assess which mode dominates SST variability in each grid cell. For models where we have multiple simulations, we take the mean across these, and we then also calculate the multi-model mean across our four models.

In the Northern Hemisphere, we find that the Greenland Mode always dominates SST (Figure 2), whilst in the Southern Hemisphere the GMOT mode is generally dominant between 30°S and 60°S. Zonal means indicate that the GMOT mode dominates at these latitudes both for the multi-model mean and for each individual model. The 13 Southern Ocean sediment cores included in the Anderson et al. (2021) compilation all lie within this latitude band. This helps verify that SST reconstructions from these cores should reflect GMOT changes across DO events. Consideration of SST proxy records from the Northern Hemisphere would not be meaningful, as Figure 2 shows these sites will be dominated by the Greenland mode and therefore unable to provide information on GMOT changes. Other latitude bands in the Southern Hemisphere are also less strongly linked to the GMOT mode, compared to the 30°S and 60°S band considered in the Anderson et al. (2021) compilation.

In order to conduct direct proxy-model comparison, we calculate SST_{SO} and $T_{Antarctic}$ for each model, following the approach of the Anderson et al. (2021) and Parrenin et al. (2013b) proxy stacks as closely as possible. To construct SST_{SO} we take the mean summer (DJF) SST within ±3° of latitude/longitude around each core site in the Anderson et al. (2021) compilation, take anomalies with respect to time, and then stack these anomalies. Although Anderson et al. (2021) include two independent SST reconstructions using different proxies from one sediment core, we choose to weight this site equally to all the others. To construct $T_{Antarctic}$, we take the annual mean surface air temperature within ±4° of latitude (±2.5° for HadCM3 due to its higher resolution) and ±5° of longitude (all models) of the five ice core sites used by Parrenin et al. (2013b), before calculating and stacking anomalies in the same manner.

For both COSMOS and HadCM3, we additionally have one isotope-enabled run which we can use to investigate the link between changes in Antarctic $\delta^{18}O$ and $T_{Antarctic}$. The details of these are given in Table 1 under "Isotope-

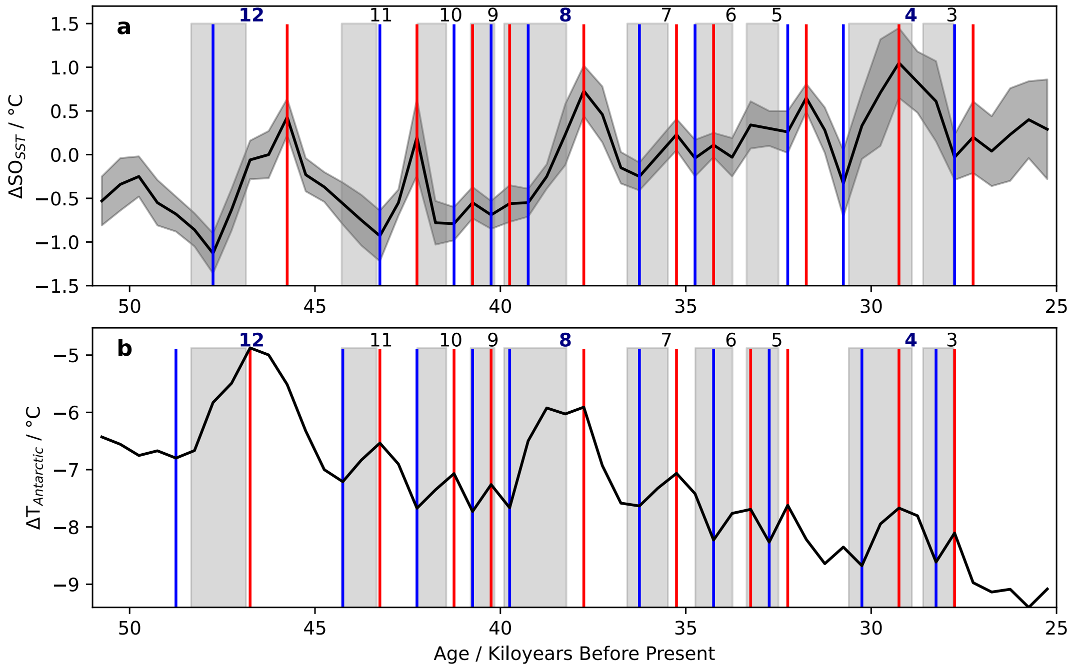

Figure 3. The peaks (red) and troughs (blue) used to calculate the warming preceding each AIM event in the Anderson et al. (2021) SST_{SO} stack (a) and the Parrenin et al. (2013b) $T_{Antarctic}$ stack (b). Stadial periods are shaded in gray, using the Rasmussen et al. (2014) stratigraphy. AIM events 3 to 12 are labeled at the end of the preceding stadial, with AIM events following Heinrich stadials labeled in bold, navy text. Note that AIM events are numbered to match the Greenland DO events that occurred approximately simultaneously (EPICA Community Members, 2006), but that the preceding stadial is therefore numbered differently, for example, AIM 3 occurs at the end of Greenland Stadial 4.

enabled Simulations." We stack δ^{18}O over the same five core sites as $T_{Antarctic}$ and calculate the gradient of the correlation between the two, known as the palaeothermometer. Both isotope-enabled simulations, but particularly that of HadCM3, initially show strong model drift (Slattery et al., 2025), and so we remove the first 800 (HadCM3) or 1500 (COSMOS) years before calculating the palaeothermometer gradient.

Finally, to understand how the changes across DO events compare with current and future changes due to anthropogenic global warming, we additionally analyse CMIP6 SSP2-4.5 simulations, using the same subset of seven models as a previous study (J. Zhu et al., 2023) for comparability. These models are CanESM5, EC-Earth3, FGOALS-g3, GFDL-ESM4, IPSL-CM6A-LR, MIROC6, and MRI-ESM2-0. We calculate SST_{SO} and $T_{Antarctic}$ in exactly the same manner as for our DO-like simulations and find the warming trends over the years 2015–2100. Although these SSP2-4.5 simulations do not contain DO-like events or any comparable abrupt changes, they provide a useful point of comparison to the better-understood present and future climate changes.

2.4. Quantifying Changes Across DO Events

In order to calculate the warming preceding each real or simulated AIM event, we follow the approach taken by Anderson et al. (2021). From their SST_{SO} stack at 500-year resolution, they identify the relevant trough and peak for each of AIM 3–12 using expert judgment and calculate the warming between these times (see Figure 3). They further propagate the stacking uncertainty to these warming values. For $T_{Antarctic}$ we follow the above approach exactly, binning the data into 500-year bins before calculating the warming for each AIM. Given the lower age uncertainty and proxy error of the ice cores used by Parrenin et al. (2013b) to generate $T_{Antarctic}$, as compared to the SST reconstructions of Anderson et al. (2021), the identification of peaks and troughs in this case is much more obvious and can therefore be automated. We do so by finding the lowest $T_{Antarctic}$ value within 0.75 kiloyears of the start of each stadial and the highest value within the same range of the end of each stadial, finally calculating the warming between these two times. Although the timing of the peaks and troughs differ somewhat between SST_{SO} and $T_{Antarctic}$, these differences are less than the age uncertainty of SST_{SO}.

For the model simulations we smooth the data over only 100 years, rather than 500 in the proxies, because we find that some oscillations would otherwise not be resolved. Using the timings of warming and cooling transitions in the NGRIP site temperature as described in Section 2.3 we identify the closest peak in GMOT, SST_{SO}, and $T_{Antarctic}$ to each Greenland warming transition and the closest trough to each Greenland cooling transition. We then use these to calculate the warming in our three variables of interest associated with each simulated AIM, starting from the first Greenland cooling transition in each simulation. Given the absence of either age uncertainty or proxy error to contend with, the identifications of peaks and troughs in these simulations can easily be made in an automated and objective manner.

The combinations of background parameters used for these simulations are somewhat arbitrary, and so for each model we have an ensemble of opportunity, not a robust exploration of the parameter space. In order to reduce the impact of this, we choose to give equal weight to each AIM event, rather than to each simulation, when calculating mean values for each model. This means that those simulations which oscillate more frequently, due to having CO_2 concentrations lying closer to the center of the “sweet-spot” of their model (Malmierca-Vallet et al., 2024), are more heavily weighted. Our model means should therefore be thought of as largely reflecting the central behavior of this oscillatory sweet-spot. Note that we never average across multiple models, only across the AIM events simulated by each individual model.

3. Results and Discussion

3.1. Simulated Patterns of Change

We are first of all interested in how the simulated GMOT, SST_{SO}, and $T_{Antarctic}$ vary over time in the four climate models. We find that these three variables are moderately well correlated in all four models, as expected based on proxies and simulations of other periods in the earth's climate history (Anderson et al., 2021; Shackleton et al., 2021; C. Zhu et al., 2024). To assess possible timing differences between the temperature peaks in GMOT, SST_{SO}, and $T_{Antarctic}$ we stack all of the AIM events in each model, aligning these events using the time of the associated abrupt Greenland warming transitions (Figures 4a–4d). In all four models, the GMOT peaks align very closely with the abrupt Greenland warming transitions, as in the examples in Figure 1. For CCSM4, we find that the peaks in SST_{SO} and $T_{Antarctic}$ occur around 100 years later than that in GMOT, in agreement with a recent study (Svensson et al., 2026). CCSM4 thus supports the hypothesis that the Southern Hemisphere warming signal originates in the subsurface Atlantic following an AMOC weakening, thus impacting GMOT first, before slowly propagating southward into the Southern Ocean and across the Antarctic Circumpolar Current, as has been previously suggested based on freshwater-forced CCSM4 simulations (Pedro et al., 2018). In HadCM3 and MPI-ESM, by contrast, the peaks all appear to occur simultaneously, whilst for COSMOS the $T_{Antarctic}$ peak alone is delayed by several hundred years compared to those in GMOT and SST_{SO}. This suggests that the dynamics in these latter three models differ somewhat from those identified in CCSM4, with rapid atmospheric teleconnections (e.g., Trombini et al., 2025) possibly playing a more important role.

While the magnitudes of the mean simulated warming preceding AIM events vary somewhat across the four models and three variables we consider, we also observe some important commonalities. Three out of our four models (CCSM4, MPI-ESM, and COSMOS) simulate the greatest warming amongst the three variables in $T_{Antarctic}$, and a different set of three out of four (CCSM4, HadCM3, and MPI-ESM) simulate the smallest warming in GMOT (Figure 4e). Across all models and variables, we find that the greatest warming is 1.23 ± 0.05°C for $T_{Antarctic}$ in CCSM4 and the smallest is 0.13 ± 0.01°C for GMOT in MPI-ESM.

A shared feature across all four models is that they simulate a mean warming in $T_{Antarctic}$ which is greater than that in GMOT. CCSM4 and MPI-ESM are consistent with the approximately three-to-one ratio of $T_{Antarctic}$ warming to GMOT warming found across proxy reconstructions of both the last deglaciation (Bereiter et al., 2018) and the last interglacial (Shackleton et al., 2020), but in HadCM3 and COSMOS this ratio is instead smaller (Figure 4f). It must be noted, however, that an appreciable part of the $T_{Antarctic}$ change on glacial-interglacial timescales is due to elevation changes in the Antarctic ice sheet (Turner et al., 2023; Werner et al., 2018). Our model simulations have fixed ice sheets, meaning that they cannot account for the impact of elevation changes on $T_{Antarctic}$. Whilst ice sheet changes are expected to be small over our timescales of interest, neglecting these may still introduce some imprecision. Nevertheless, these results may suggest that CCSM4 and MPI-ESM better simulate the relative temperature changes in Antarctica and the global ocean.

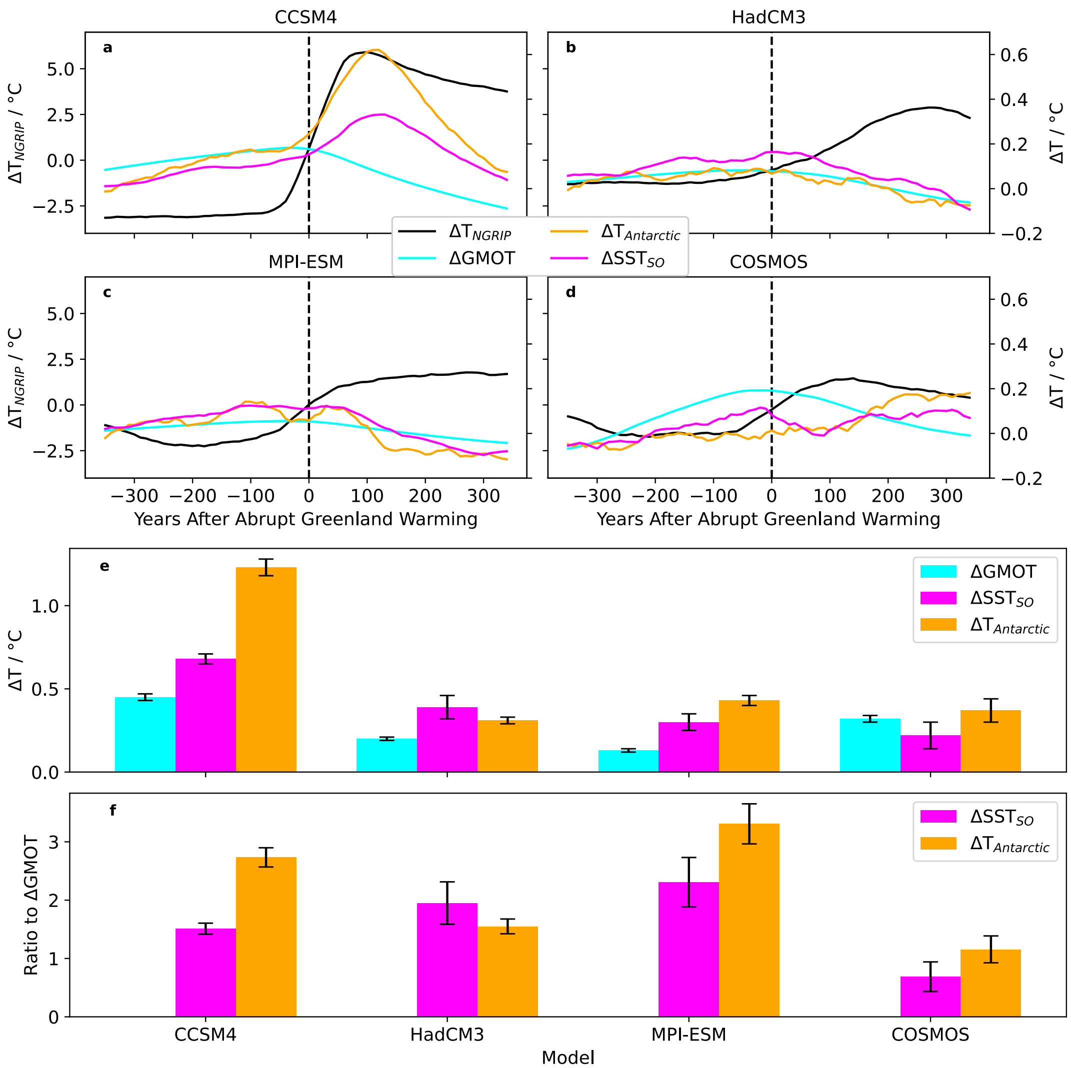

Figure 4. Stacked temperature over all simulated AIM events in CCSM4 (a), HadCM3 (b), MPI-ESM (c), and COSMOS (d) for the 350 years before and after an abrupt Greenland warming transition. T_{NGRIP} is on the left-hand scale, whilst GMOT, SST_{SO}, and $T_{Antarctic}$ are all on the right-hand scale. Also shown are the mean AIM warming in GMOT (cyan), SST_{SO} (magenta), and $T_{Antarctic}$ (orange) for each model, with 1σ errors (e), and the mean AIM warming in SST_{SO} (magenta), and $T_{Antarctic}$ (orange) for each model expressed as a ratio of the mean GMOT warming, again with 1σ errors (f).

3.2. Proxy-Model Comparison

Previous analyses of SST_{SO} (Anderson et al., 2021) and $T_{Antarctic}$ (EPICA Community Members, 2006) have found a clear correlation between the magnitude of warming associated with an AIM event and the duration of the preceding stadial. It is therefore necessary to take this trend into account when making a comparison between the model simulations and proxy reconstructions. When we do so, we find that the combination of mean AIM warming and mean stadial duration for each of our models falls with the 95% uncertainty range of the proxy trend for both SST_{SO} and $T_{Antarctic}$, as seen in Figure 5, but that many of the individual simulated AIM events do not. This is primarily because in the models the observed trend of increasing warming with increasing stadial duration is either missing (HadCM3 and COSMOS), severely underestimated (MPI-ESM), or apparent only after controlling for the dominant effect of background CO_2 concentration. This last situation is the case for CCSM4, where the simulations with higher CO_2 produce a cluster of AIM events (seen upper left in Figure 5b) with both shorter stadial durations and greater warming magnitudes, obscuring the much smaller impact of duration on warming. Despite this largely missing trend, the fact that the model means agree with the proxy evidence is a

10.1029/2026PA005582

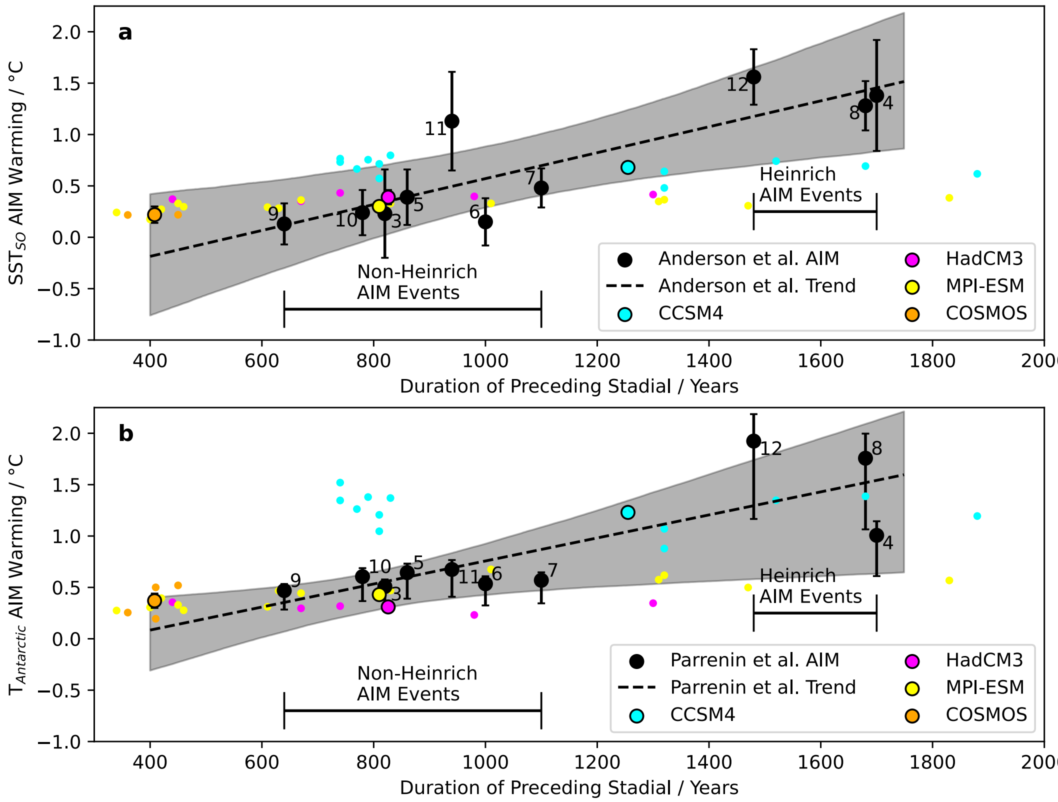

Figure 5. The trend of SST$_{SO}$ (a) and T$_{Antarctic}$ (b) AIM warming against the duration of the preceding stadial for AIM events 3 to 12 using proxy reconstructions, with shading showing the 95% uncertainty range. Also shown are the AIM warming and duration for individual AIM events in each of the four models (small colored circles) and the model means (larger colored circles). The error bars for SST$_{SO}$ represent the 1σ random stacking error, whilst for T$_{Antarctic}$ they represent the full range of the systematic error due to the choice of palaeothermometer, meaning that the errors on T$_{Antarctic}$ warming are not independent (see Appendix B for details). Note that one AIM event from CCSM4 is not shown, due to a stadial duration of more than 3,000 years, but is still included in the model mean.

validation of these models and shows that, when in their oscillatory sweet spots with respect to CO_2 concentration (Malmierca-Vallet et al., 2024), they accurately simulate plausible AIM events.

Of the AIM events in MIS3, events 4, 8, and 12 follow stadials which contain Heinrich events and which are both markedly longer than the other stadials in MIS3 and also generally have greater AIM warming (Figure 5). These events are additionally associated with notable increases in atmospheric CO_2 (Henry et al., 2016). We thus refer to AIMs 4, 8, and 12 as "Heinrich AIM events" and to the others as "non-Heinrich AIM events." AMOC strength is believed to have dramatically declined during Heinrich events due to freshwater input into the North Atlantic, as opposed to a more partial weakening during other stadials (Henry et al., 2016). Despite this, Anderson et al. (2021) suggest that the greater Southern Ocean warming of Heinrich AIM events is solely due to the longer duration of their preceding stadials, as in their stack the SST$_{SO}$ warming values for Heinrich and non-Heinrich AIM events fall on the same trend line. However, for both Anderson et al. (2021) SST$_{SO}$ and Parrenin et al. (2013b) T$_{Antarctic}$ there is no significant trend within the subset of either Heinrich or non-Heinrich AIM events, such that the observed trend is only significant due to the difference between these two groups.

An alternate interpretation is therefore that there is not a continual trend of greater AIM warming with greater stadial duration, but instead two distinct regimes, with the greater warming of Heinrich AIM events and the longer durations of their preceding stadials both being results of the more drastic reduction in AMOC strength. In particular, the greater warming of Heinrich AIM events may be due in part to the large increases in atmospheric CO_2 during Heinrich stadials. This interpretation is supported by the negligible or non-existent trends of AIM warming with stadial duration in the four models (Figure 5). Arguing against this interpretation, however, are the overlap (considering uncertainties) of the proxy AIM warming values for the two groups in Figure 5 and the fact

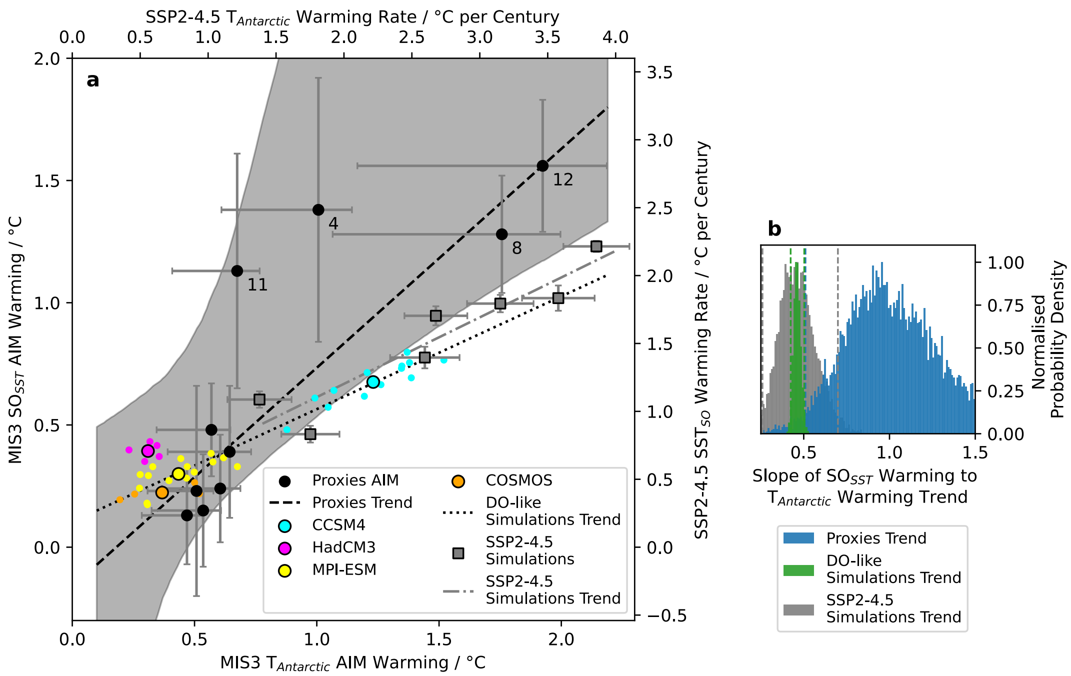

Figure 6. (a) The slope of SST_{SO} warming against $T_{Antarctic}$ warming for AIM events 3–12 in the Anderson et al. (2021) and Parrenin et al. (2013b) proxy stacks (black circles, with the 95% confidence interval of the trend in gray), individual AIM events from our DO-like model simulations (colored circles), and 21st century warming rate in CMIP6 SSP2-4.5 simulations (gray squares). Model means for the DO-like simulations are shown with black outlines. As in Figure 5, the errors on $T_{Antarctic}$ warming are systematic and not independent. Note also that the SSP2-4.5 warming rates are plotted on different axes to the MIS3 proxies and simulations, however the trends remain comparable. (b) Probability distributions (normalized to have a maximum value of one) for the slopes of SST_{SO} warming against $T_{Antarctic}$ warming for the proxies (blue), DO-like simulations (green), and SSP2-4.5 simulations (gray), with the bounds of their central 95% ranges indicated with vertical lines. These probability distributions are calculated by bootstrapping, propagating all uncertainties (see Appendix B for further details).

that other proxy reconstructions have indeed shown clear correlations between duration and warming within the two groups (e.g., EPICA Community Members, 2006).

All of the oscillations in the model simulations we consider are spontaneous and not driven by any freshwater forcing. In this sense they are more comparable to the non-Heinrich AIM events as recorded by proxies, and less comparable to the meltwater-amplified Heinrich AIM events. If the Heinrich and non-Heinrich events are indeed two entirely separate regimes, then comparing proxy records of Heinrich AIM events to our DO-like simulations would not be valid, and we should not expect these to agree. Given the available proxy evidence, it is unfortunately not possible to conclude whether the two categories of AIM events differ only in magnitude or whether they do in fact fundamentally differ in kind. We thus continue to cautiously compare our simulated DO-like oscillations to both the Heinrich and non-Heinrich events in proxy records.

Figure 5 shows that the model means are generally closer to the non-Heinrich than the Heinrich AIM events in terms of stadial duration and the magnitude of warming in both SST_{SO} and $T_{Antarctic}$, with HadCM3 and MPI-ESM fitting particularly well within this cluster. CCSM4 is somewhat of an exception, sitting between the Heinrich and non-Heinrich AIM events and with the shape of its $T_{Antarctic}$ warming better matching the Heinrich AIM events (Svensson et al., 2026), but COSMOS is equally an outlier in the opposite direction, simulating a shorter mean stadial duration than even the shortest observed in MIS3. By demonstrating that the oscillations simulated by all models other than CCSM4 only match the non-Heinrich events we are able to explain why a previous proxy-model comparison study (Slattery et al., 2025), which was unable to distinguish between Heinrich and non-Heinrich events due to dating uncertainties in their proxies, found the models to significantly underestimate the observed changes.

Turning next to the slopes of the correlations between SST_{SO} warming and $T_{Antarctic}$ warming, we find a discrepancy between the models and proxies (Figure 6). When applying a linear regression to the Anderson et al. (2021) and Parrenin et al. (2013b) proxy stacks we find that the residuals are not normally distributed ($p < 0.05$ using a Shapiro-Wilk test), and so the linear regression is not valid in this case. Instead, we use robust regression with Huber's T loss function, which gives less weight to outliers such as AIM events 4, which has unusually small Antarctic warming for a Heinrich AIM event, and 11, which has an unusually large Southern Ocean warming for a non-Heinrich AIM event (Figure 6). We thus find a slope of 0.9 (95% uncertainty range 0.5–4.0), which is surprisingly large given the widely observed pattern of greater warming over land than ocean (Byrne & O'Gorman, 2013, 2018), although it is important to note that the framework that explains this pattern has not been validated at high latitudes and so may not hold for Antarctica and the Southern Ocean.

After splitting up the DO-like model simulations into their individual AIM events, we find that only CCSM4 and MPI-ESM show a significant positive correlation between the AIM warming in SST_{SO} and $T_{Antarctic}$, and so we calculate an overall trend (labeled "DO-like Simulations Trend" in Figure 6) using only AIM events from these two models. Returning to standard linear regression, the resulting slope of 0.46 ± 0.04 is extremely similar to the slope of 0.49 (95% range 0.25–0.70) found for the twenty-first century warming rates in the SSP2-4.5 simulations. The SSP2-4.5 simulations show relatively linear global warming over less than a century, as opposed to the non-linear regional warming over several centuries seen for the DO-like simulations. This makes the agreement between the two regarding the slope of SST_{SO} warming to $T_{Antarctic}$ warming even more striking, and highlights the discrepancy with the slope found for the proxies.

Despite the large uncertainty range for the slope of the proxies, with the upper bound being particularly poorly constrained, the lower bound of the 95% uncertainty range is larger than the central estimates for the slopes seen in both the DO-like or SSP2-4.5 model simulations. When comparing the probability distributions for the slopes of the proxies and the DO-like simulations, there is no overlap between their respective central 95% ranges (Figure 6b), indicating that the discrepancy or disagreement between the proxies and models is robust. We therefore investigate possible reasons for this proxy-model discrepancy in the Appendices (Appendices A–C), finding that a positive bias in the Anderson et al. (2021) SST_{SO} warming due to proxy noise and age uncertainty is likely a contributor.

3.3. Implications for MIS3 GMOT Variation

Combining all of our analysis of the proxies and model simulation enables us to comment on the likely true magnitude of GMOT warming across AIM events in MIS3, even in the absence of a specific proxy reconstruction. We have found in Section 3.2 that the model-means for stadial duration, SST_{SO} warming, and $T_{Antarctic}$ warming are broadly comparable to those observed in proxy records of the non-Heinrich AIM events during MIS3. It is therefore likely that the true GMOT warming across these non-Heinrich events is in the range given by the model means for GMOT warming in Figure 4 of 0.1–0.5°C, including uncertainties.

GMOT variability of this magnitude would be difficult to resolve in an ice core reconstruction of GMOT as it is comparable to the measurement error, given as 0.2°C (1σ) by Shackleton et al. (2021), but it nonetheless may be possible to do so if a large number of samples can be combined so as to improve the signal-to-noise ratio. This is the case for the Shackleton et al. (2021) reconstruction preceding AIM 19 at the beginning of MIS5, which shows a suggestive (though not statistically significant) GMOT warming of 0.3 ± 0.3°C (1σ). However, this cannot easily be compared to our model simulations because changes in ocean circulation are believed to have altered the response to abrupt climate change between MIS5 and MIS3 (Thornalley et al., 2013).

To attempt to estimate the GMOT warming preceding Heinrich AIM events in MIS3, we investigate the relationships of GMOT warming to SST_{SO} and $T_{Antarctic}$ warming in the models (Figure 7). Considering individual simulated AIM events, only CCSM4 and MPI-ESM show significant correlations in both cases, linked to the fact that these are also the two models that show a significant correlation between warming in SST_{SO} and $T_{Antarctic}$ as discussed in Section 3.2. We again calculate trends from these two models, which we can then use to extrapolate from the modeled GMOT changes to those one might expect for Heinrich AIM events.

Here, however, the issue of the discrepancy between the simulated and observed slopes of SST_{SO} to $T_{Antarctic}$ warming presents a challenge. Using the model trend of GMOT warming against SST_{SO} warming, in combination with the range of SST_{SO} warming for Heinrich AIM events in the Anderson et al. (2021) stack, suggests an approximate range of GMOT warming for these Heinrich AIM events of 0.9–1.2°C. Meanwhile, the same

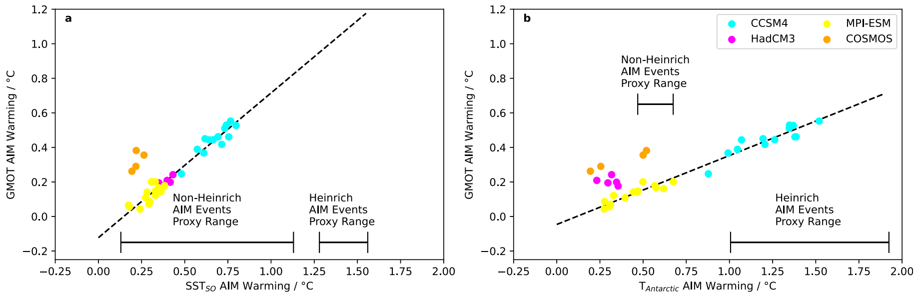

Figure 7. The relationship across individual simulated AIM events in our four models of GMOT warming against SO_{SST} warming (a) and GMOT warming against $T_{Antarctic}$ warming (b). The trends shown are for the AIM events in CCSM4 and MPI-ESM only. The observed ranges for SO_{SST} and $T_{Antarctic}$, based on the proxy evidence, are shown separately for non-Heinrich and Heinrich AIM events.

approach using the model and proxy warmings in $T_{Antarctic}$ instead leads to a range of 0.4–0.7°C, which is in clear disagreement.

The best evidence of GMOT warming preceding a larger AIM event in the last glacial is again from Shackleton et al. (2021), in this case for AIM 17 at the boundary of MIS4 and MIS3. Their reconstruction, which only partially covers this period, indicates warming of 1.0 ± 0.3°C (1σ). Given the uncertainty, this would not rule out either the higher estimate from SST_{SO} or the lower one from $T_{Antarctic}$, even ignoring the complications of the wider climate changes occurring at the time of AIM 17, including those in ice sheet extent (and thus sea level) and CO_2 concentrations (Shackleton et al., 2021). We therefore cannot discriminate between our two contradictory estimates for the GMOT warming of Heinrich AIM events in MIS3, and so our best estimate must combine both into the extremely broad range of 0.4–1.2°C. At the very least, we can confidently state that these changes across Heinrich AIM events would definitely be resolvable in an ice core GMOT reconstruction, and so that such a reconstruction would be a worthwhile endeavor.

4. Conclusions

Through analysis of climate model simulations showing spontaneous, Dansgaard–Oeschger like oscillations, we have confirmed that Global Mean Ocean Temperature varies according to the bipolar seesaw (Pedro et al., 2018), with peaks in GMOT coinciding with DO warming events in Greenland and troughs with DO cooling events. We have also confirmed that these GMOT changes are smaller than the strongly-correlated changes in Antarctic temperature, as seen in proxy reconstructions over longer timescales. This provides partial validation of the simulated GMOT changes in these models.

Accounting for the previously noted link between stadial duration and warming magnitude, we find that the mean values of simulated warming for Southern Ocean SST and Antarctic Temperature in each model agree well with previously-published proxy compilations. This proxy-model comparison also demonstrates that most of these models reproduce only the non-Heinrich DO/AIM events (i.e., those that follow stadials without Heinrich events), as has been hypothesized previously (Slattery et al., 2025; Zhang et al., 2021). This further explains why a previous proxy-model comparison study, where the distinction between Heinrich and non-Heinrich events was not possible, found some of these same models to underestimate the observed changes (Slattery et al., 2025). Using this match between the simulations and the proxy records of non-Heinrich AIM events, we estimate that GMOT change for the non-Heinrich AIM events in MIS3 is likely to fall in the range 0.1–0.5°C.

Of the four models investigated, CCSM4 and MPI-ESM show consistently significant correlations between the magnitudes of warming in GMOT, SST_{SO}, and $T_{Antarctic}$, demonstrating greater skill than COSMOS and HadCM3 in simulating these changes. However, the slopes of these correlations differ notably between proxies and models, with this discrepancy proving robust despite the large uncertainties in the proxy reconstructions. We identify a positive bias in the SST_{SO} proxy warming which likely causes part of this observed proxy-model discrepancy. This leads to contradictory estimates of the GMOT warming preceding Heinrich AIM events when extrapolating the model trends, and so we are able only to make a conservative estimate of 0.4–1.2°C. We further note that it is unclear whether Heinrich and non-Heinrich AIM events are distinct categories or represent different regions along a continuum—a distinction which has important consequences for the validity of such an extrapolation. Targeted simulations of both spontaneous and freshwater-forced DO-like events in the same models, following the Malmierca-Vallet et al. (2023) protocols, would help to address this outstanding question, and so we highlight this as an area for future work. Detailed analysis and comparison of the mechanisms by which the Southern Ocean and Antarctic warmings occur in the different models would also be extremely valuable in helping to resolve the remaining uncertainties surrounding the bipolar thermal seesaw in response to DO events.

Given that our estimate for the GMOT changes of non-Heinrich AIM events in MIS3 is comparable to the measurement error of ice core-derived reconstructions, resolving these changes would likely prove very challenging. We would therefore propose that any future MIS3 GMOT reconstruction should not simply aim to cover the whole period but should instead initially prioritize the periods around the Heinrich AIM events 4, 8, and 12, which we are confident could be resolved. This would be extremely valuable, as it would not only provide a novel test of the DO-like model simulations but also serve to validate the existing proxy records for SST_{SO} and $T_{Antarctic}$, due to their strong links. Where sufficient ice core samples are available, subsequent work could then target GMOT across particular non-Heinrich AIM events, taking measurements from replicate samples so as improve the signal/noise ratio sufficiently in order to resolve these changes too. Only then will we truly be able to know whether model simulations accurately reproduce the variability of this key component of the climate system.

Appendix A: Bias in SST_{SO} Proxy AIM Warming

We firstly consider potential biases in the construction of the Anderson et al. (2021) SST_{SO} stack and Parrenin et al. (2013b) $T_{Antarctic}$ stack. Anderson et al. (2021) create age scales for their 14 SST records based on AIM events that are identified using expert judgment. In doing so, they generally associate the largest observed warming events in these records with the Heinrich AIM events 4, 8, and 12. Whilst this is a reasonable approach, given that these Heinrich AIM events generally show greater warming in other proxies such as Antarctic ice cores (e.g., EPICA Community Members, 2006; Landais et al., 2021), it is possible that some warming peaks may have been assigned erroneously, creating one potential source of bias in SST_{SO}. It is impossible to objectively determine which warming events in SST proxy records correspond to which AIMs, however, and so we cannot quantify this source of bias.

We next consider the impacts of the large proxy errors and dating uncertainties of the individual records on the calculation of the warming magnitude of each AIM. We create "pseudo-proxies" under two scenarios, making different assumptions about the true underlying signal. In the first case, we assume that there is no signal and that the observed SST_{SO} warming is solely due to over-interpreted noise. In the second, we assume that the true underlying signal of each SST record is $T_{Antarctic}$, scaled to half its magnitude (approximately matching the model slopes in Figure 6) and with the orbital-scale cooling trend removed, as this trend is not present in SST_{SO} (see Figure 3). In both cases, we then interpolate this signal (or lack thereof) to the ages of the data points in each SST proxy record, incorporating age uncertainty, and add white noise with standard deviation matching the proxy error given by Anderson et al. (2021). We combine these pseudo-proxy records into 500-year bins and stack them to give a synthetic SST_{SO} stack before calculating the warming associated with each AIM event as described in Section 2.4 and finally finding the slope against $T_{Antarctic}$. Repeating this 10,000 times, we generate distributions of the slope of SST_{SO} against $T_{Antarctic}$ given our two assumptions, which are shown in Figure A1.

In the first case (Figure A1a), when we assume that there is no underlying signal in SST_{SO}, the distribution of simulated slopes is shifted toward positive values, indicating bias due to the process of stacking and calculation of SST_{SO} warmings. Nonetheless, the slope observed between the proxies is greater than any simulated under this assumption, demonstrating that the observed correlation between SST_{SO} warming and $T_{Antarctic}$ warming is statistically significant with respect to this null distribution. When we instead assume an underlying signal with half the magnitude of $T_{Antarctic}$ (Figure A1b), we again find that the distribution of simulated slopes is shifted toward positive values, from an assumed underlying slope of 0.5 to a mean simulated slope of 0.66. We find that this increase compared to the assumed slope is due in approximately equal parts to the removal of the orbital-scale cooling trend on one hand and the combined effect of proxy error, age uncertainty, and the stacking procedure on the other.

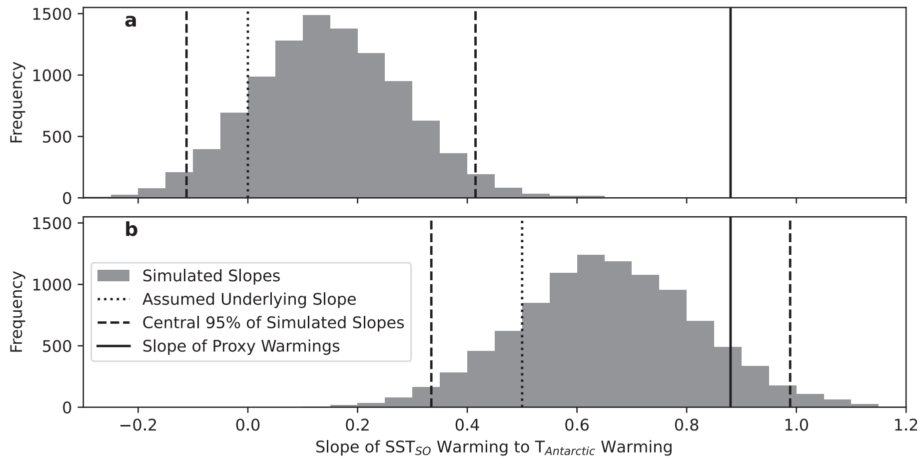

Figure A1. Distributions for the slope of SST$_{SO}$ warming against T$_{Antarctic}$ warming, assuming (a) that there is no underlying signal in SST$_{SO}$, and (b) that the underlying signal in SST$_{SO}$ is simply T$_{Antarctic}$ with the magnitude halved and orbital-scale cooling removed. The observed slope in the proxies is shown with a full vertical line, the bounds of the central 95% of the simulated distribution are shown with dashed lines, and the assumed underlying slope is shown with a dotted line.

This analysis shows clear evidence of a positive bias in the slope of SST$_{SO}$ to T$_{Antarctic}$ AIM warming. Given this bias, as well as the wide uncertainty caused by the relatively large proxy noise in the SST records, the observed slope of 0.88 is consistent with our second assumption of an underlying signal with half the magnitude of T$_{Antarctic}$, because the observed slope for the proxies lies comfortably within the 95% range of the distribution of simulated slopes in Figure A1b. Overall, we can conclude that the observed correlation between SST$_{SO}$ and T$_{Antarctic}$ AIM warming is statistically significant, but also that the slope of this correlation has likely been exaggerated by the effect of the positive bias shown here, contributing to the discrepancy between the proxy and model slopes seen in Figure 6.

Having found this positive bias affecting the AIM warming in SST$_{SO}$, we can estimate what the slope between the proxies for SST$_{SO}$ and T$_{Antarctic}$ would be without it. For each AIM event in MIS3, we calculate the bias as the percentage difference between the mean simulated warming for the "pseudo-proxies" and the assumed underlying warming, following our second assumption of an underlying signal with half the magnitude of T$_{Antarctic}$. We then further assume each of the AIM warmings in the Anderson et al. (2021) SST$_{SO}$ stack have been inflated by this same percentage difference, and calculate a "corrected" value by removing these estimates of the bias for each AIM. It is important to note that this approach depends heavily on the assumptions we have made here, and so our "corrected" values for SST$_{SO}$ warming should be considered illustrative, rather than definitive. Figure A2 shows that this illustrative bias correction brings the proxy and model slopes into agreement, within uncertainty, further demonstrating that the observed discrepancy is largely driven by the bias in SST$_{SO}$ warming.

Although this bias correction would also imply a lower SST$_{SO}$-derived estimate for GMOT warming for Heinrich AIM events in MIS3, agreeing much more so with that derived from T$_{Antarctic}$, this is highly circular given our assumption that the underlying signal in SST$_{SO}$ follows T$_{Antarctic}$ with a slope consistent with the models. Whilst we therefore refrain from altering our previously stated range of 0.4–1.2°C, we would still note that the upper end of this estimate is less likely when considering the bias we have discussed here.

10.1029/2026PA005582

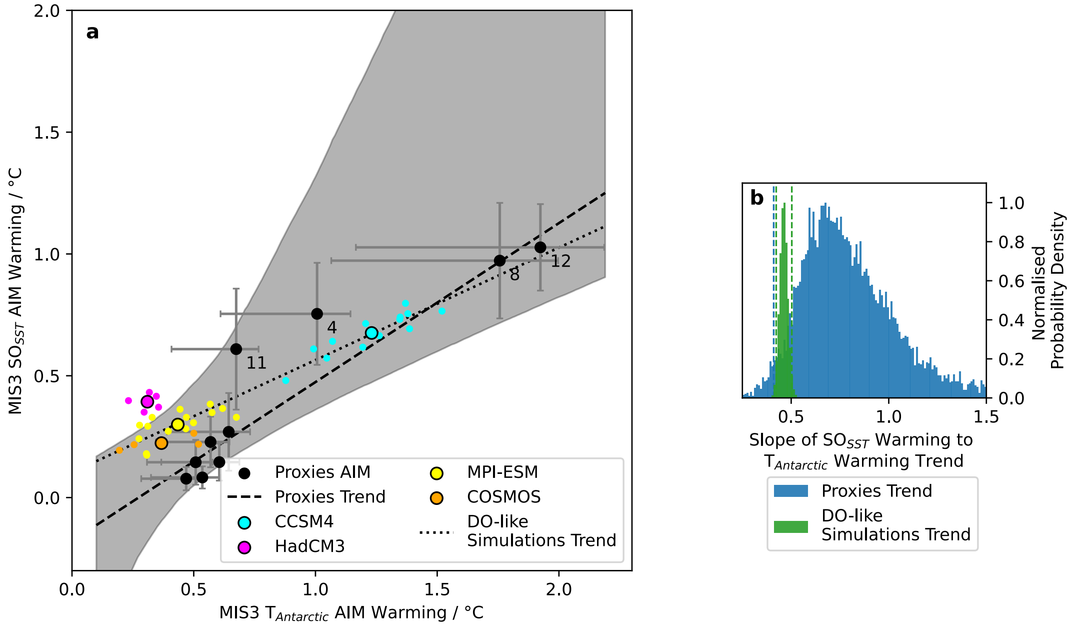

Figure A2. (a) As for Figure 6, but with the SST$_{SO}$ warming "corrected" for the positive bias we have identified. Error bars for SST$_{SO}$ now show 1σ of a normally distributed random error in the magnitude of bias, which is propagated to the probability distribution for the "Proxies" slope in (b). As in Figures 5 and 6, the errors on T$_{Antarctic}$ warming are systematic and not independent.

Appendix B: Uncertainties in T$_{Antarctic}$ Proxy AIM Warming

The largest uncertainty affecting the Parrenin et al. (2013b) T$_{Antarctic}$ stack is the systematic uncertainty in the palaeothermometer gradient used to convert the isotope records into temperature. Parrenin et al. (2013b) use a value of 1.32°C/‰, taken from a spatial traverse over East Antarctica and verified with simple modeling. Isotope-enabled climate models can help to constrain the true value of the palaeothermometer, but two recent studies comparing simulations of the LGM and the PI (Buizert et al., 2021; Werner et al., 2018) yield notably different results. Based on these studies, we take a conservative approach and assume a uniform uncertainty distribution between 0.8 and 1.5°C/‰, whilst continuing to use the Parrenin et al. (2013b) value of 1.32°C/‰for our best estimates, leading to asymmetric uncertainties in T$_{Antarctic}$ as seen in Figures 5 and 6. We propagate these uncertainties assuming perfectly correlated errors for T$_{Antarctic}$ warming across different AIM events, implying a fixed palaeothermometer gradient across the duration of MIS3. Despite the large uncertainty this leads to in our estimate of the slope for the proxies, the discrepancy compared to the slope of the DO-like simulations is robust as the overlap between the two probability distributions is less than 2% (Figure 6b).

We also assess the palaeothermometer gradient ourselves, using the isotope-enabled DO-like simulations from HadCM3 and COSMOS, which are a more direct comparison to the proxies than present-day spatial regressions or estimates based on LGM simulations. When we compare stacked T$_{Antarctic}$ and δ^{18}O, we find gradients of 0.7 ± 0.2°C/‰for HadCM3 (2σ uncertainty), although this should be interpreted carefully in light of the strong drift in this simulation, and 0.9 ± 0.4°C/‰for COSMOS. Both models would therefore point to a smaller palaeothermometer gradient than used by Parrenin et al. (2013b). However, adopting a smaller value for the palaeothermometer gradient on this evidence would only worsen the proxy-model discrepancy, as seen in Figure B1. In light of this, we choose not to alter the Parrenin et al. (2013b) T$_{Antarctic}$, continuing to use their choice of 1.32°C/‰.

For the proxy and model slopes in Figure 6 to agree, in the absence of any other changes, we would have to convert δ^{18}O to temperature using a palaeothermometer gradient of ~2.6°C/‰, which is well above any estimate we are aware of. Although uncertainty in this value is an important source of uncertainty in the T$_{Antarctic}$ warming, it therefore seems highly unlikely that this is the reason for the observed proxy-model discrepancy. A more promising candidate for this is the choice taken by Parrenin et al. (2013b) to "*rescale the temperature*

10.1029/2026PA005582

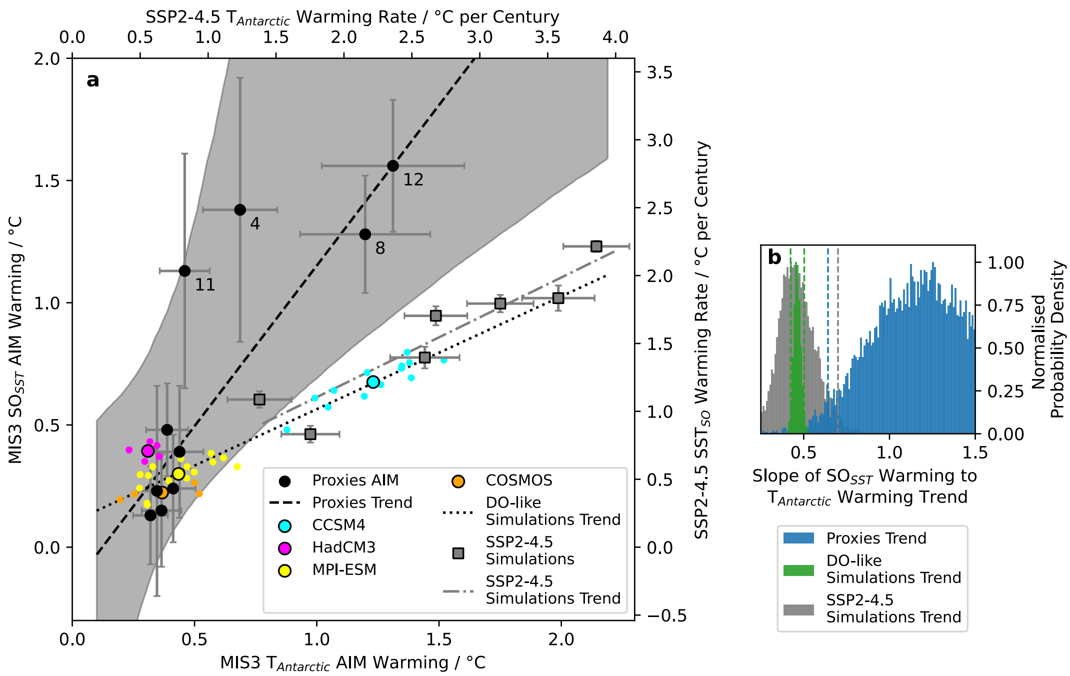

Figure B1. (a) As for Figure 6, but with the $T_{Antarctic}$ warming and uncertainties rescaled based on the palaeothermometer gradient found in the COSMOS isotope-enabled DO-like simulation. Error bars for $T_{Antarctic}$ now show 1σ of a normally distributed systematic error, which has been propagated to the probability distribution for the "Proxies" slope in (b). Once again, the errors on $T_{Antarctic}$ warming are systematic and not independent.

reconstruction from each ice core so that the resulting ΔT has the same average and standard deviation than the EDC one on the interval 0–140 kyr b1950." This rescaling based on the glacial-interglacial variability could reduce the magnitude of $T_{Antarctic}$ warming across AIMs if other core sites show less variability than EDC at millennial timescales, relative to the glacial-interglacial timescale. This is therefore a potential contributor to bias in the SST_{SO} to $T_{Antarctic}$ slope, although its impact is much less than certain than that of the bias identified in Appendix A.

Appendix C: Impact of Seasonality

The Anderson et al. (2021) SST proxies are thought to reflect summer temperatures, whilst the Parrenin et al. (2013b) Antarctic temperature stack is considered an annual mean. This differing seasonality complicates our analysis, and could contribute to the discrepancy seen between the proxies and models in Figure 6. To test the impact of this, we compare the AIM warming in our standard SST_{SO} in the DO-like simulations (taking the mean over December, January, and February) with an alternate version which is identical except for being an annual mean. We find that the summer (DJF) SST_{SO}, as we use elsewhere in this study, shows somewhat greater AIM warming than the annual mean SST_{SO} in CCSM4, whilst in the other models these are similar. Using all individual AIM events in CCSM4 and MPI-ESM (as for Figures 6 and 7), we find a trend between the DJF and annual mean SST_{SO} AIM warming of 1.10 ± 0.04 (2σ) as seen in Figure C1.

This analysis shows that, in these models, the Southern Ocean SST warms more in summer preceding than during the rest of the year. It is possible that the size of this difference between the DJF and annual means is underestimated in the models and that during MIS3 the Southern Ocean warming was even more so accentuated during the austral summer. This could possibly explain why the proxy trend in Figure 6 shows (summer) SST_{SO} warming increasing almost as fast as (annual) $T_{Antarctic}$ warming. However, whilst this is a compelling hypothesis, there are unfortunately no independent annual mean SST_{SO} records available with which we might be able to test it. The impact of differing seasonality on the proxy/model comparison is therefore unquantifiable, but it is nonetheless a potentially important contribution to the observed discrepancy between the proxies and models.

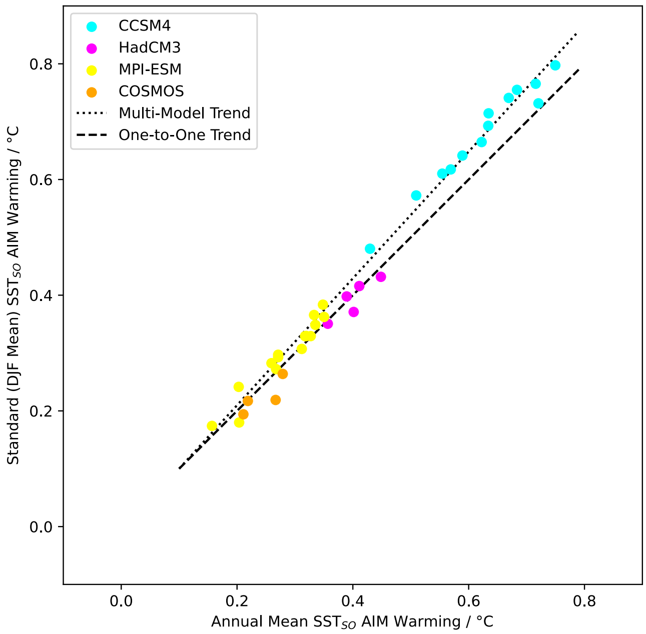

Figure C1. The warming of individual AIM events in our four models for both the standard (DJF) and annual mean versions of SST_{SO}. The dotted line shows the multi-model trend, using AIM events from CCSM4 and MPI-ESM, whilst the dashed line shows a one-to-one trend, that is, with equal warming in both versions of SST_{SO}.

Conflict of Interest

The authors declare no conflicts of interest relevant to this study.

Availability Statement

The Southern Ocean Sea Surface Temperature Stack (Anderson et al., 2020) is available at https://doi.org/10.1594/PANGAEA.912158. The Antarctic Temperature Stack (Parrenin et al., 2013a) is available at https://doi.org/10.1594/PANGAEA.810188. The DO-like model data are available from https://www.bas.ac.uk/project/sdoo. CMIP6 data are available at https://esgf-ui.ceda.ac.uk/search from the Earth System Grid Federation (ESGF).

Acknowledgments

This work was funded by the European Union's Horizon Europe research and innovation programme under Past-to-Future (P2F): Towards fully paleo-informed future climate projections (P2F), GN 101184070. JS was additionally supported by a NERC C-CLEAR-DTP studentship. LCS and IMV were additionally supported NERC-KANG-GLAC, GN NE/V006509/1, and LCS was also supported by: NERC-SWAIS2C, GN NE/X009386/1; Reflections-RADTIP, GN RE-1002; and MBIE Antarctic Sea Ice Switch-ASIS, GN RSCHTRUSTVIC 2448. FM was supported by a NERC Discovery Science Grant (NE/W006243/1).

References

Anderson, H. J., Pedro, J. B., Bostock, H. C., Chase, Z., & Noble, T. L. (2020). Southern Ocean sea surface temperature anomaly stacks [Dataset]. *PANGAEA*. https://doi.org/10.1594/PANGAEA.912158

Anderson, H. J., Pedro, J. B., Bostock, H. C., Chase, Z., & Noble, T. L. (2021). Compiled Southern Ocean sea surface temperatures correlate with Antarctic Isotope Maxima. *Quaternary Science Reviews*, *255*, 106821. https://doi.org/10.1016/j.quascirev.2021.106821

Armstrong, E., Izumi, K., & Valdes, P. (2022). Identifying the mechanisms of DO-scale oscillations in a GCM: A salt oscillator triggered by the Laurentide ice sheet. *Climate Dynamics*, *60*(11–12), 3983–4001. https://doi.org/10.1007/s00382-022-06564-y

Baggenstos, D., Häberli, M., Schmitt, J., Shackleton, S. A., Birner, B., Severinghaus, J. P., et al. (2019). Earth's radiative imbalance from the Last Glacial Maximum to the present. *Proceedings of the National Academy of Sciences*, *116*(30), 14881–14886. https://doi.org/10.1073/pnas.1905447116

Bereiter, B., Shackleton, S., Baggenstos, D., Kawamura, K., & Severinghaus, J. (2018). Mean global ocean temperatures during the last glacial transition. *Nature*, *553*(7686), 39–44. https://doi.org/10.1038/nature25152

Brown, N., & Galbraith, E. D. (2016). Hosed vs. unhosed: Interruptions of the Atlantic meridional overturning circulation in a global coupled model, with and without freshwater forcing. *Climate of the Past*, *12*(8), 1663–1679. https://doi.org/10.5194/cp-12-1663-2016

Buizert, C., Fudge, T. J., Roberts, W. H. G., Steig, E. J., Sherriff-Tadano, S., Ritz, C., et al. (2021). Antarctic surface temperature and elevation during the Last Glacial Maximum. *Science*, *372*(6546), 1097–1101. https://doi.org/10.1126/science.abd2897

Byrne, M. P., & O'Gorman, P. A. (2013). Land–ocean warming contrast over a wide range of climates: Convective quasi-equilibrium theory and idealized simulations. *Journal of Climate*, *26*(12), 4000–4016. https://doi.org/10.1175/JCLI-D-12-00262.1

Byrne, M. P., & O'Gorman, P. A. (2018). Trends in continental temperature and humidity directly linked to ocean warming. *Proceedings of the National Academy of Sciences*, *115*(19), 4863–4868. https://doi.org/10.1073/pnas.1722312115

Capron, E., Rasmussen, S. O., Popp, T. J., Erhardt, T., Fischer, H., Landais, A., et al. (2021). The anatomy of past abrupt warmings recorded in Greenland ice. *Nature Communications*, *12*(1), 2106. https://doi.org/10.1038/s41467-021-22241-w

Cortese, G., & Abelmann, A. (2002). Radiolarian-based paleotemperatures during the last 160 kyr at ODP Site 1089 (Southern Ocean, Atlantic Sector). *Palaeogeography, Palaeoclimatology, Palaeoecology*, *182*(3), 259–286. https://doi.org/10.1016/S0031-0182(01)00499-0

Crosta, X., Sturm, A., Armand, L., & Pichon, J.-J. (2004). Late Quaternary sea ice history in the Indian sector of the Southern Ocean as recorded by diatom assemblages. *Marine Micropaleontology*, *50*(3), 209–223. https://doi.org/10.1016/S0377-8398(03)00072-0

Dansgaard, W., Johnsen, S. J., Clausen, H. B., Dahl-Jensen, D., Gundestrup, N. S., Hammer, C. U., et al. (1993). Evidence for general instability of past climate from a 250-kyr ice-core record. *Nature*, *364*(6434), 218–220. https://doi.org/10.1038/364218a0

EPICA Community Members. (2006). One-to-one coupling of glacial climate variability in Greenland and Antarctica. *Nature*, *444*(7116), 195–198. https://doi.org/10.1038/nature05301

Grimmer, M., Baggenstos, D., Schmitt, J., Krauss, F., Shackleton, S., Severinghaus, J. P., & Fischer, H. (2025). AMOC modulates ocean heat content during deglaciations. *Geophysical Research Letters*, *52*(6), e2024GL114415. https://doi.org/10.1029/2024GL114415

Hemming, S. R. (2004). Heinrich events: Massive late Pleistocene detritus layers of the North Atlantic and their global climate imprint. *Reviews of Geophysics*, *42*(1). https://doi.org/10.1029/2003RG000128

Henry, L. G., McManus, J. F., Curry, W. B., Roberts, N. L., Piotrowski, A. M., & Keigwin, L. D. (2016). North Atlantic Ocean circulation and abrupt climate change during the last glaciation. *Science*, *353*(6298), 470–474. https://doi.org/10.1126/science.aaf5529

Kindler, P., Guillevic, M., Baumgartner, M., Schwander, J., Landais, A., & Leuenberger, M. (2014). Temperature reconstruction from 10 to 120 kyr b2k from the NGRIP ice core. *Climate of the Past*, *10*(2), 887–902. https://doi.org/10.5194/cp-10-887-2014

Klockmann, M., Mikolajewicz, U., Kleppin, H., & Marotzke, J. (2020). Coupling of the subpolar gyre and the overturning circulation during abrupt glacial climate transitions. *Geophysical Research Letters*, *47*(21), e2020GL090361. https://doi.org/10.1029/2020GL090361

Klockmann, M., Mikolajewicz, U., & Marotzke, J. (2018). Two AMOC states in response to decreasing greenhouse gas concentrations in the coupled climate model MPI-ESM. *Journal of Climate*, *31*(19), 7969–7984. https://doi.org/10.1175/JCLI-D-17-0859.1

Kuniyoshi, Y., Abe-Ouchi, A., Sherriff-Tadano, S., Chan, W.-L., & Saito, F. (2022). Effect of climatic precession on Dansgaard-Oeschger-like oscillations. *Geophysical Research Letters*, *49*(6), e2021GL095695. https://doi.org/10.1029/2021GL095695

Landais, A., Stenni, B., Masson-Delmotte, V., Jouzel, J., Cauquoin, A., Fourré, E., et al. (2021). Interglacial Antarctic–Southern Ocean climate decoupling due to moisture source area shifts. *Nature Geoscience*, *14*(12), 918–923. https://doi.org/10.1038/s41561-021-00856-4

Li, C., & Born, A. (2019). Coupled atmosphere-ice-ocean dynamics in Dansgaard-Oeschger events. *Quaternary Science Reviews*, *203*, 1–20. https://doi.org/10.1016/j.quascirev.2018.10.031

Lisiecki, L. E., & Raymo, M. E. (2005). A Pliocene-Pleistocene stack of 57 globally distributed benthic $\delta^{18}O$ records. *Paleoceanography*, *20*(1). https://doi.org/10.1029/2004PA001071

Lynch-Stieglitz, J. (2017). The Atlantic meridional overturning circulation and abrupt climate change. *Annual Review of Marine Science*, *9*(1), 83–104. https://doi.org/10.1146/annurev-marine-010816-060415

Malmierca-Vallet, I., Sime, L. C., & the D–O community members. (2023). Dansgaard–Oeschger events in climate models: Review and baseline Marine Isotope Stage 3 (MIS3) protocol. *Climate of the Past*, *19*(5), 915–942. https://doi.org/10.5194/cp-19-915-2023

Malmierca-Vallet, I., Sime, L. C., Valdes, P. J., Klockmann, M., Vettoretti, G., & Slattery, J. (2024). The impact of CO_2 and climate state on whether Dansgaard–Oeschger type oscillations occur in climate models. *Geophysical Research Letters*, *51*(13), e2024GL110068. https://doi.org/10.1029/2024GL110068

North Greenland Ice Core Project Members. (2004). High-resolution record of Northern Hemisphere climate extending into the last interglacial period. *Nature*, *431*(7005), 147–151. https://doi.org/10.1038/nature02805

Parrenin, F., Masson-Delmotte, V., Köhler, P., Raynaud, D., Paillard, D., Schwander, J., et al. (2013b). Synchronous change of atmospheric CO_2 and Antarctic temperature during the last deglacial warming. *Science*, *339*(6123), 1060–1063. https://doi.org/10.1126/science.1226368

Parrenin, F., Masson-Delmotte, V., Köhler, P., Raynaud, D., Paillard, D., Schwander, J., et al. (2013a). Antarctic temperature stack (ATS) from five different ice cores (EDC, Vostok, Dome Fuji, TALDICE, and EDML) [Dataset]. *PANGAEA*. https://doi.org/10.1594/PANGAEA.810188

Pedro, J. B., Andersson, C., Vettoretti, G., Voelker, A. H. L., Waelbroeck, C., Dokken, T. M., et al. (2022). Dansgaard-Oeschger and Heinrich event temperature anomalies in the North Atlantic set by sea ice, frontal position and thermocline structure. *Quaternary Science Reviews*, *289*, 107599. https://doi.org/10.1016/j.quascirev.2022.107599

Pedro, J. B., Jochum, M., Buizert, C., He, F., Barker, S., & Rasmussen, S. O. (2018). Beyond the bipolar seesaw: Toward a process understanding of interhemispheric coupling. *Quaternary Science Reviews*, *192*, 27–46. https://doi.org/10.1016/j.quascirev.2018.05.005

Rasmussen, S. O., Bigler, M., Blockley, S. P., Blunier, T., Buchardt, S. L., Clausen, H. B., et al. (2014). A stratigraphic framework for abrupt climatic changes during the Last Glacial period based on three synchronized Greenland ice-core records: Refining and extending the INTIMATE event stratigraphy. *Quaternary Science Reviews*, *106*, 14–28. https://doi.org/10.1016/j.quascirev.2014.09.007

Shackleton, S., Baggenstos, D., Menking, J. A., Dyonisius, M. N., Bereiter, B., Bauska, T. K., et al. (2020). Global ocean heat content in the Last Interglacial. *Nature Geoscience*, *13*(1), 77–81. https://doi.org/10.1038/s41561-019-0498-0

Shackleton, S., Bereiter, B., Baggenstos, D., Bauska, T. K., Brook, E. J., Marcott, S. A., & Severinghaus, J. P. (2019). Is the noble gas-based rate of ocean warming during the younger dryas overestimated? *Geophysical Research Letters*, *46*(11), 5928–5936. https://doi.org/10.1029/2019GL082971

Shackleton, S., Menking, J. A., Brook, E., Buizert, C., Dyonisius, M. N., Petrenko, V. V., et al. (2021). Evolution of mean ocean temperature in Marine Isotope Stage 4. *Climate of the Past*, *17*(5), 2273–2289. https://doi.org/10.5194/cp-17-2273-2021

Sikes, E. L., O'Leary, T., Nodder, S. D., & Volkman, J. K. (2005). Alkenone temperature records and biomarker flux at the subtropical front on the Chatham rise, SW Pacific Ocean. *Deep Sea Research Part I: Oceanographic Research Papers*, *52*(5), 721–748. https://doi.org/10.1016/j.dsr.2004.12.003

Sikes, E. L., & Sicre, M.-A. (2002). Relationship of the tetra-unsaturated C37 alkenone to salinity and temperature: Implications for paleoproxy applications. *Geochemistry, Geophysics, Geosystems*, *3*(11), 1–11. https://doi.org/10.1029/2002GC000345

Sikes, E. L., & Volkman, J. K. (1993). Calibration of alkenone unsaturation ratios (*U*k'37) for paleotemperature estimation in cold polar waters. *Geochimica et Cosmochimica Acta*, *57*(8), 1883–1889. https://doi.org/10.1016/0016-7037(93)90120-L

Slattery, J., Sime, L. C., Rehfeld, K., Weitzel, N., Malmierca-Vallet, I., Zhang, X., et al. (2025). A global speleothem-based assessment of spontaneous Dansgaard–Oeschger type oscillations in two isotope-enabled general circulation models. *Geophysical Research Letters*, *52*(18), e2025GL114906. https://doi.org/10.1029/2025GL114906

Stocker, T. F., & Johnsen, S. J. (2003). A minimum thermodynamic model for the bipolar seesaw. *Paleoceanography*, *18*(4). https://doi.org/10.1029/2003PA000920

Svensson, A., Vettoretti, G., Lin, J.-M., Sinnl, G., Dahl-Jensen, D., Steffensen, J. P., et al. (2026). Bipolar volcanic ice-core synchronization of the entire last glacial period. *Quaternary Science Reviews*, *375*, 109755. https://doi.org/10.1016/j.quascirev.2025.109755

Ternois, Y., Sicre, M.-A., Boireau, A., Beaufort, L., Miquel, J.-C., & Jeandel, C. (1998). Hydrocarbons, sterols and alkenones in sinking particles in the Indian Ocean sector of the Southern Ocean. *Organic Geochemistry*, *28*(7), 489–501. https://doi.org/10.1016/S0146-6380(98)00008-4

Thornalley, D. J. R., Barker, S., Becker, J., Hall, I. R., & Knorr, G. (2013). Abrupt changes in deep Atlantic circulation during the transition to full glacial conditions. *Paleoceanography*, *28*(2), 253–262. https://doi.org/10.1002/palo.20025

10.1029/2026PA005582

Trombini, I., Weitzel, N., Valdes, P. J., Baudouin, J.-P., Armstrong, E., & Rehfeld, K. (2025). Atmospheric and Oceanic pathways drive separate modes of Southern Hemisphere climate in simulations of spontaneous Dansgaard-Oeschger-type oscillations. *Geophysical Research Letters*, *52*(5), e2024GL111473. https://doi.org/10.1029/2024GL111473

Turner, F. E., Buck, C. E., Jones, J. M., Sime, L. C., Vallet, I. M., & Wilkinson, R. D. (2023). Reconstructing the Antarctic ice-sheet shape at the Last Glacial Maximum using ice-core data. *Journal of the Royal Statistical Society - Series C: Applied Statistics*, *72*(5), 1493–1511. https://doi.org/10.1093/jrsssc/qlad078

Vettoretti, G., Ditlevsen, P., Jochum, M., & Rasmussen, S. O. (2022). Atmospheric CO_2 control of spontaneous millennial-scale ice age climate oscillations. *Nature Geoscience*, *15*(4), 300–306. https://doi.org/10.1038/s41561-022-00920-7

Vettoretti, G., Hu, R.-J., Bethke, I., Krüger, K., Sigl, M., Outten, S., et al. (2026). Volcanism-induced collapse and recovery of the Atlantic meridional overturning circulation under glacial conditions. *Science Advances*, *12*(6), eadx2124. https://doi.org/10.1126/sciadv.adx2124

Werner, M., Jouzel, J., Masson-Delmotte, V., & Lohmann, G. (2018). Reconciling glacial Antarctic water stable isotopes with ice sheet topography and the isotopic paleothermometer. *Nature Communications*, *9*(1), 3537. https://doi.org/10.1038/s41467-018-05430-y

Zhang, X., Barker, S., Knorr, G., Lohmann, G., Drysdale, R., Sun, Y., et al. (2021). Direct astronomical influence on abrupt climate variability. *Nature Geoscience*, *14*(11), 819–826. https://doi.org/10.1038/s41561-021-00846-6

Zhu, C., Sanchez, S., Liu, Z., Clark, P. U., He, C., Wan, L., et al. (2024). Enhanced ocean heat storage efficiency during the last deglaciation. *Science Advances*, *10*(38), eadp5156. https://doi.org/10.1126/sciadv.adp5156

Zhu, C., Zhang, J., Liu, Z., Otto-Bliesner, B. L., He, C., Brady, E. C., et al. (2022). Antarctic warming during Heinrich Stadial 1 in a transient isotope-enabled deglacial simulation. *Journal of Climate*, *35*(22), 7353–7365. https://doi.org/10.1175/JCLI-D-22-0094.1

Zhu, J., Xie, A., Qin, X., & Xu, B. (2023). Assessment of future Antarctic amplification of surface temperature change under different Scenarios from CMIP6. *Journal of Mountain Science*, *20*(4), 1074–1089. https://doi.org/10.1007/s11629-022-7646-5